An integrated dielectrophoretic chip for continuous bioparticle filtering, focusing, sorting, trapping, and detecting

I-Fang Cheng and Hsien-Chang Chang[a)]
Institute of Nanotechnology and Microsystem Engineering, Institute of Biomedical Engineering, National Cheng Kung University, Tainan, Taiwan, Republic of China

Diana Hou and Hsueh-Chia Chang[b)]
Center for Microfluidics and Medical Diagnostics, Department of Chemical and Biomolecular Engineering, University of Notre Dame, Notre Dame, Indiana 46556

(Received 21 December 2006; accepted 1 March 2007; published online 10 May 2007)

Multi-target pathogen detection using heterogeneous medical samples require continuous filtering, sorting, and trapping of debris, bioparticles, and immunocolloids within a diagnostic chip. We present an integrated AC dielectrophoretic (DEP) microfluidic platform based on planar electrodes that form three-dimensional (3D) DEP gates. This platform can continuously perform these tasks with a throughput of 3 μL/min. Mixtures of latex particles, *Escherichia coli Nissle, Lactobacillus*, and *Candida albicans* are sorted and concentrated by these 3D DEP gates. Surface enhanced Raman scattering is used as an on-chip detection method on the concentrated bacteria. A processing rate of 500 bacteria was estimated when 100 μl of a heterogeneous colony of 10^7 colony forming units /ml was processed in a single pass within 30 min. © *2007 American Institute of Physics.*
[DOI: 10.1063/1.2723669]

I. INTRODUCTION

Typically, biomedical samples contain a mixture of debris, bacteria, and other organisms, creating a heterogeneous matrix of bioparticles. In order to isolate the target pathogen from this matrix, expensive and large laboratory equipment must be used, such as a centrifuge. The centrifuge can effectively separate undesired materials that differ in size and mass, but bioparticles are similar in size and composition and require higher speeds and longer centrifugation times. However, at these speeds, cells and bacteria can be damaged or ripped open due to the strong centrifugal force needed for this type of separation. Once the target pathogen is isolated, the concentrations are typically low and require time-consuming culturing steps to reach concentrations high enough for detection. Despite the time and labor costs for centrifuging and culturing samples, these methods still remain the gold standards for pathogen detection. Modern immunoassay techniques, like agglutination, utilize antibody functionalized immunocolloids to trap or detect specific bacteria, thus, eliminating or reducing culturing requirements. Lab-on-a-chip devices strive to integrate and miniaturize these bioparticle filtering, sorting, trapping, and detecting processes into a continuous-flow chip-scale device that can reduce labor and equipment needs, and yet process a realistic sample volume (>10 μl) within a reasonable duration (<1 h). For a typical medical sample with more than one million bacteria/ml, this translates into a need for processing more than 10 bacteria/s.

Current sorting technologies for integrated chips typically use electrokinetic and hydrodynamic forces on the particle.[1] They rely on the principle that, with the same applied electric or

a)Electronic mail: hcchang@mail.ncku.edu.tw; Telephone: +886-6-275-7575, ext. 63426
b)Electronic mail: hchang@nd.edu; Telephone: 574-631-5697

flow field, different pathogens experience different particle forces and can then be directed to different positions on the chip. For example, field flow fractionation is based on the differences in the size or density of the bioparticle, therefore, it is insensitive to bacteria that are roughly of the same size and density. A particular electrokinetic method that is pathogen sensitive and is not damaging to the bioparticle itself is AC dielectrophoresis.[2–4] A particle in a nonuniform electric field will form an induced dipole based on the relative permittivity of the particle and the surrounding medium. The movement of the particle to regions of high/low field due to this induced polarization is termed dielectrophoresis (DEP).[5] A bioparticle's DEP effects are highly sensitive to the dimension, shape, conductivity, and permittivity of the cell interior and cell membrane, which vary widely for different species, live/dead, and diseased bacteria/cells. Moreover, this selective sensitivity can be tuned by adjusting the AC frequency and the conductivity of the solution.[6–8] For example, live and dead bacteria have been shown to migrate by DEP forces to different regions on the chip at the same frequency because of the change in their ion channel activity. DEP separation by size and shape of the bacteria can be adjusted by altering the condition of the medium or by forming conductivity gradients.[9–11]

Continuous-flow DEP devices that have been used to sort cells include electrical field flow fractionation (E-FFF),[12] trapezoidal electrode arrays,[13] and DEP deflection.[14] However, as the DEP traps are typically planar electrodes, their field gradient penetration depth is limited by the electrode gap. More importantly, the field intensity gradient is mostly in the direction normal to the through-flow and, therefore, cannot be used effectively to counter Stokes drag. As a result, these inefficient DEP traps and sorters require long channels and low flow rates, thus, severely limiting the throughput. Recent work has tried to overcome the low trapping efficiency of planar DEP traps and sorters by combining hydrodynamic and electrokinetic methods to sort bacteria. Optical detection is used to actively direct the flow to specific channels, and a pinched flow fractionization design has been reported.[15] However, the insensitivity of cells, bacteria, and viruses to hydrodynamic sorting effects still reduce the selectivity of these faster devices. Using a series of interdigitated castellated electrodes, alternating flow directions and electrode activation can separate live/dead yeast cells in a continuous flow system.[16] However, due to the drop-off of the DEP force in the bulk with respect to the electrode surface and the scaling of the particle radius with relation to the DEP force, $\sim r^3$, a small particle can only be affected by DEP when it is in close proximity of the electrode surface.

DEP has also been used to concentrate bacteria, but the speed of this process is again limited by the short range and normal field gradient direction of planar DEP electrodes. By combining a converging flow field near the stagnation point of an internal recirculation flow driven by AC electro-osmosis, longer-range and faster trapping onto planar electrodes can be achieved.[7,17,18] However, a robust through-flow would still severely limit their trapping efficiency.

A promising solution to the low efficiency of planar DEP traps in through-flow is to use a three-dimensional (3D) electrode system, where the electrodes are fabricated on the top and bottom of the channel.[19,20] The 3D configuration produces a DEP gate, whose field spans the entire height of the channel, and whose field gradient and DEP force (field intensity gradient) is exactly against the flow direction. These gates, used in a continuous flow device, can be used to direct and deflect particles to specific regions on the chip or trap the particles.[19,21–26] However, the alignment and bonding of the top and bottom electrodes is difficult and has prevented many DEP techniques from adapting to this configuration. The aligning can be done using a microscope, however, the bonding of the chip once the electrodes are aligned creates additional difficulties. Bonding the chips by heat is undesirable because the electrodes and the chip would be removed from the microscope causing the alignment to shift. Gluing the electrodes together also is difficult because along with aligning, excess glue can contaminate the channel or an unevenly coated surface will cause some areas to be glued, while others are not. Thus, using planar electrodes on one side of the chip is less time-consuming and is often used in DEP chips. To our knowledge, due to these technical obstacles, an integrated 3D DEP chip for continuous filtering, focusing, sorting, and trapping of bacteria has not been reported in the literature.

After the bacteria are sorted and concentrated, their identity must be determined by an on-chip

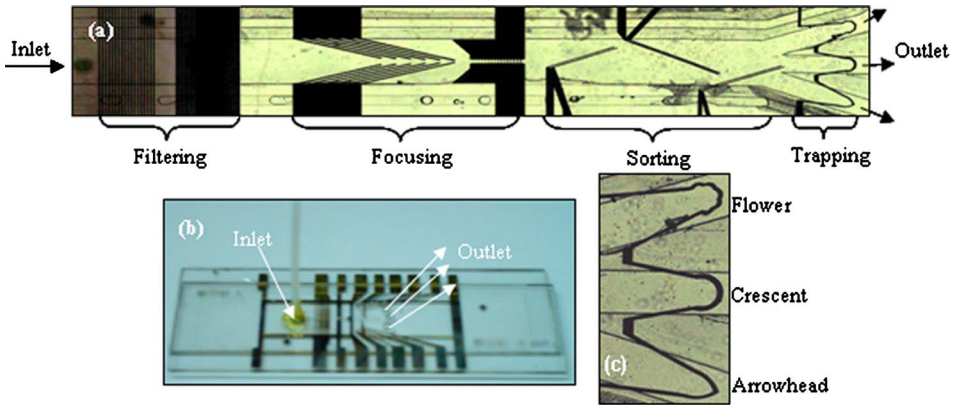

FIG. 1. (a) Image of the four stages of the integrated chip from the inlet to outlet. (b) The entire chip consists of a 25 μm high, 1 mm wide, and 14.5 mm long channel, enclosed by two glass slides. The individual outlet channels are 25 μm high, 350 μm wide, and 5.5 mm in length. Electrodes were fabricated on both glass slides, creating a 3D electrode system. (c) A top view of the three different trapping electrode configuration. From the top channel to the bottom channel, a flower—multiple curved electrode, crescent—a semicircle electrode, and an arrowhead—a pointed electrode.

or an external sensor. For lab-on-a-chip devices, the current identification methods include micro-PCR, impedance, and immunocolloids.[27–29] While impedance spectroscopy cannot offer species identification, it can quantify the amount of bacteria that are trapped.[28] For immunoassays, micron and nanometer sized particles are functionalized with antibodies to be used as immunocolloids. However, to reduce the transport time for colloid-pathogen docking, a large number of immunocolloids must be utilized. Thus, the sorting and detection of colloids with and without docked pathogens then becomes the technological challenge. Micro-PCR can identify the species but it is unable to quantify and detect live/dead cells. Fluorescence labeling and specific genetic sequence labeling have also been used as detection methods.[30] However, these methods require multiple steps to prepare the sample for detection, such as washing, separating, and setting specific temperature sequences. These preparatory sequences create additional processing steps that need to be developed for an on-chip device. In contrast, a detection method that has minimal preparatory sequences and has been used for on-chip detection is spectroscopy, such as infrared (IR), ultraviolet and visible (UV-Vis) and Raman spectroscopy.[31–33] IR and Raman spectroscopy measure the vibrational modes of the molecules and the various structures, thus providing a detailed spectrum.[34] In particular, Raman spectroscopy can often show bonds that are undetectable through IR, thus, it has been shown to be extremely specific to each bacterium, where each spectrum can act as a *fingerprint*.[35] Additionally, no preparatory steps are needed for Raman spectroscopy and the sample can be scanned, while the bacteria are concentrating. Recent advances and applications have shown the range of characterization abilities for Raman detection of amino acids, DNA, bacteria, live/dead yeast cells, and tumor/nontumor cells.[36–38] Raman scattering is a very weak effect, where only 1 in 10^6 photons that scatter result in Raman scatter,[34] thus, high concentrations of bacteria are required for detection. Advances in Raman spectroscopy have led to the development of surface enhanced Raman scattering (SERS).[39,40] SERS uses a mixture of the sample and metal nanoparticle ($\sim$80–100 nm) to enhance the intensity of the Raman scatter of the molecule. The metal nanoparticles must be either chemically bonded to the bacteria or settle in the proximity of the bacteria in order to increase the scattering. This advancement has allowed for more detailed spectra at lower concentrations and faster scanning times. Currently, the fastest scanning time reported is 20 s, however, high bacteria concentrations were used.[41] Chemical agents and nucleic material have also been further characterized using SERS.[42–45]

In this study, we designed an integrated chip (see Fig. 1) that allowed continuous flow bioparticle filtering, focusing, sorting, trapping, and detecting by using 3D DEP forces and SERS. The bioparticles were sorted by deflecting them into individual channels by angled electrodes based on their negative DEP mobilities. In the individual channels, a negative DEP electrode gate

was used to trap and concentrate the sorted bioparticles for further detection by SERS. The frequency ranges of positive and negative DEP were found experimentally for each bacterium so that they could be sorted based on these frequencies. Different DEP trap geometries, shown in Fig. 1(c), were examined and an arrowhead design was found to be the optimal. Latex particles, *Candida albicans*—a sepsis-causing yeast cell, *E. coli Nissle* and *Lactobacillus*—gastrointestinal bacteria, were focused, sorted, and trapped with this integrated chip. As the bacteria were trapped, their Raman spectrum was taken simultaneously and enhanced by the addition of silver nanoparticles. About 100 μl samples were processed in 30 min corresponding to the analysis of about 500 particles/s.

II. ELECTRODE DESIGN AND LAYOUT

A. DEP gating for sorting and trapping

We used a high-frequency AC field such that there was little double layer screening at the electrode and the force from the DEP electrodes was more effective.[17] Thus, we operated at frequencies above 1 MHz. However, the DEP force on the particle must be negative for the electrodes to deflect the particles toward channels on the chip and thus requires careful design and selection of operating conditions. Under a nonuniform AC electric field, a particle that is more easily polarized than the surrounding medium will be attracted toward the region of highest field. However, if the particle is less polarized than the medium, the particle will be repelled from the high field region. This attraction toward the high field region is termed positive dielectrophoresis (pDEP), while the repulsion from the high field region is termed negative dielectrophoresis (nDEP).[5] The time averaged DEP force $F_{\mathrm{DEP}}=2\pi\varepsilon_m r^3 \mathrm{Re}[f_{\mathrm{CM}}]\nabla|E|^2$ is dependent on the permittivity of the medium ε_m, the radius of the particle r, the Clausius-Mossotti (CM) factor f_{CM}, and the magnitude of the electric field gradient $\nabla|E|^2$. If the value of $\mathrm{Re}[f_{\mathrm{CM}}]$ is positive, the particle exhibits positive DEP properties and if the value of the $\mathrm{Re}[f_{\mathrm{CM}}]$ is negative, the particle exhibits negative DEP properties. However, if $f_{\mathrm{CM}}=0$, the corresponding frequency defines the crossover frequency, where the particle exhibits neither + nor − DEP properties. The CM factor is defined by $f_{\mathrm{CM}}=(\varepsilon_p^*-\varepsilon_m^*)/(\varepsilon_p^*+2\varepsilon_m^*)$, where ε_p^* and ε_m^* are the complex permittivities of the particle and the medium, respectively, and can be defined as $\varepsilon^*=\varepsilon-i\sigma/\omega$, where σ is the conductivity of the medium and ω is the frequency of the applied field. It is clear that the permittivity effects dominate at high frequencies and the conductivity effects dominate at relatively low frequencies. The permittivity of cells is typically higher than that of the medium and, therefore, undesirable pDEP typically occurs at frequencies higher than 1 MHz. To remedy this, we employed a high-conductivity buffer, much higher than the particle conductivity, to produce a very high cross-over frequency such that nDEP was still observed at the highest frequencies ($<$10 MHz) of commercial power supplies. As such, there was little double-layer screening of the electric field and yet the particles still exhibited nDEP.

Under the nDEP working conditions we employed, where the frequency was far lower than the cross-over frequency, the CM factor was real and roughly $f_{\mathrm{CM}}=-0.5$. Using the electrode width w (which is typically 30 μm) to estimate the lateral field penetration length and V/d to estimate the field, where V is the peak-to-peak voltage and d the channel height, the DEP force on any particle can be estimated as $F_{\mathrm{DEP}}=-\pi\varepsilon_m r^3(V/d)^2/w$ that acts in the direction normal to the electrode edge.

Consider a particle that has been trapped by an oblique gate with an inclination angle of θ, as shown in Fig. 2(a). Since we are considering a nDEP gate, the same electrode configuration is located on the top and the bottom of the channel. However, for simplicity we only consider a 2D case, where we have a top view of the chip to study the effect of the shape of the nDEP electrode gates. The particle cannot penetrate the gate and pass through the channel due to the DEP force but can translate along the edge of the gate toward the tip at the center. The Stokes drag on the particle, which is in the flow direction, must be countered by the projection of the DEP force in the flow direction $F_{\mathrm{DEP}}\sin\theta$. To arrest penetration across the gate, the linear flow velocity must be lower than the critical value of $v_c=\varepsilon_m r^2(V/d)^2 \sin\theta/6w\eta$. For a particle with a radius of 1 μm, an

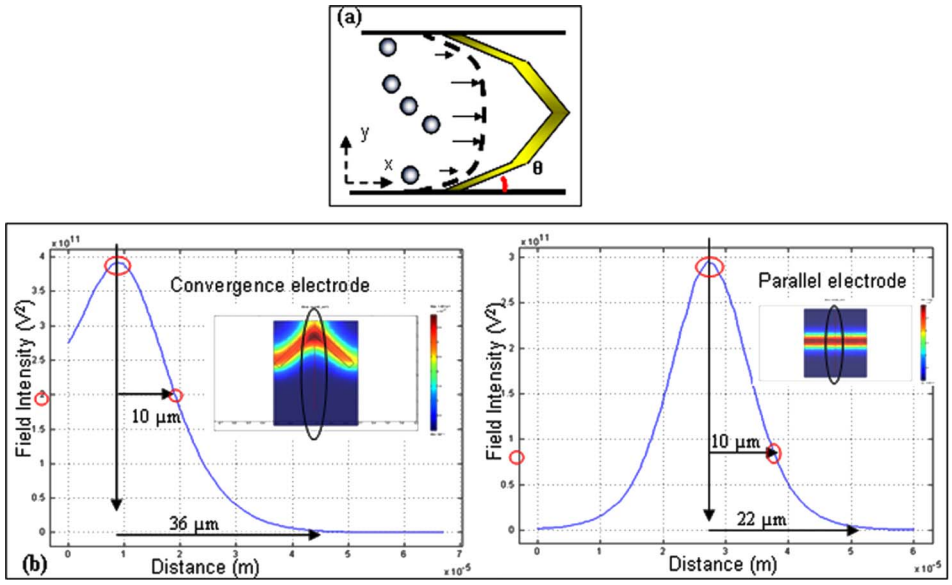

FIG. 2. (a) Flow profile of Hele-Shaw flow in the chip, due to the branch channel dimensions, 350 μm wide and 25 μm high. The angle θ of the electrode trap exploits the low viscous forces near the side wall due to the flow profile to exert a strong negative DEP force on the particles. (b) Finite element simulation on the electric field at the arrowhead tip in comparison with the electric field using a horizontal electrode. The electrode and channel geometries are the same as the actual chip and the applied voltage is 10 $V_{p\text{-}p}$. The field intensity at the midplane and at the center of the channel is shown for the two geometries.

applied field of 10 $V_{p\text{-}p}$, a channel height of 25 μm, an electrode width of 30 μm, and an inclination angle of 45°, the corresponding critical velocity is roughly 1.7 mm/s. This corresponds to the linear velocity in the flow direction at the normal position of the particle. If the particle transit time (l/v), where l is the length of the channel and v the average liquid linear velocity, is much smaller than the sedimentation time, $t_{\text{sed}}=d/v_{\text{sed}}$, then the relevant velocity is roughly the average linear liquid velocity or the velocity at the middle of the channel. Otherwise, the particles would settle to the bottom of the chip and reduce the particle throughput. This imposes the condition that $v \ll (l/d)v_{\text{sed}}$ for settling to be negligible, where the sedimentation velocity $v_{\text{sed}}=2r^2\Delta\rho g/9\eta$ ($\sim$0.1 μm/s) is negligible for micron and submicron particles despite the large aspect ratio (l/d) $\sim 10^3$. Larger debris with significant settling can however be readily filtered as they experience a lower drag at the bottom of the channel. Thus, the velocities, v_c and $(l/d)v_{\text{sed}}$, bound the operating velocities of the chip. We have designed our chip to operate at roughly 1 mm/s.

The critical velocity decreases with inclined gates. However, for the sorter electrodes with an oblique angle of about 45°, the critical velocity was only reduced by a factor of $1/\sqrt{2}$. More problematic was the trap design of Fig. 2(a), where a larger inclination must be introduced to concentrate the particles in the middle of the channel and a much lower velocity must be used. However, a slot velocity profile decays rapidly in a boundary layer of thickness d near the side walls. Hence, the largest inclination can be introduced within these side boundary layers, as shown in Fig. 2(a). Beyond the boundaries, the inclination should be reduced to about $\theta \sim 45°$ to prevent leakage and yet produce a healthy migration to the tip of the electrode.

The design of the tip of the trap can also be optimized. It is known that electric field lines tend to be compressed near corners, so much so that even infinitely high fields and field gradients are possible near sharp corners.[46] In Fig. 2(b), 3D finite element simulation of the Laplace equation for an arrowhead and a horizontal electrode geometry show a much higher field for the sharp arrow head geometry. The simulation was done under the conditions of deionized (DI) water, $\varepsilon \sim 80$, where the applied field to the electrodes was $V \sim 20$ $V_{p\text{-}p}$. The field penetration depth of 36 μm versus 22 μm, beyond the 30 μm wide electrode was nearly twice as high for the arrowhead design. This suggests an enhanced DEP force at the tip that can be used to collect more

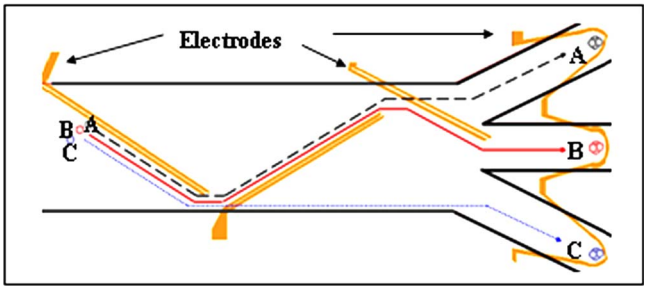

FIG. 3. A diagram of the sorting electrodes to separate particles A, B, and C by their negative DEP mobilities into individual channels. The first pair of electrodes deflects all particles, the second pair deflects only particles A and B, and the third pair deflects only particle B.

particles with the arrowhead design. The constant-potential condition on the electrode was justifiable because at the 1 MHz frequency we use, there was very little double layer screening at the electrode.[17]

B. Chip layout

The entire integrated chip contained a single channel with a height of $d=25$ μm, width of $W=1$ mm, and a length of $l=2$ cm from inlet to outlet hole, shown in Figs. 1(a) and 1(b) labeled with the four different stages: filtering, focusing, sorting, and trapping. The first parallel arrays of planar electrodes near the inlet were used to filter debris from the sample by removing particles that exhibit pDEP. This design is similar to interdigitated electrodes that are used in DEP separation.[11] However, we use a 3D gate, where the electrodes are on the top and bottom of the channel to enhance the trapping in the entire height of the channel. If these particles were left in the sample, they would be attracted to the electrodes and become a barrier for other particles by distorting the flow field and the electric field. As the mixture passed through the array, pDEP particles were attracted and trapped to the electrode while nDEP particles passed through the electrode array. The second stage contains two types of planar electrodes used for focusing.[21,47] Both electrodes used nDEP force to direct the particles toward the center of the channel. The first pair was used as a coarser focusing unit, which brought the particles from the entire 1 mm channel to a width of 50 μm, while the second interdigitated electrodes was used for a finer focusing process and brought the particles to a region of 20 μm, which formed a single line of particles. Such a focusing section is important as each particle to be processed must be sorted under identical environments. As the flow field and the electric field vary over the channel, the particles should ideally be focused to the same spot to produce effective sorting.

Once the particles were focused toward the center of the channel, they were sorted into three individual channels by three oblique DEP gates that did not span the entire channel.[19,48] They directed and deflected the bacteria to specific channels by using nDEP conditions specific to each bacterium, as shown in the diagram in Fig. 3. At the first electrode, all the particles were deflected by the oblique electrode, but at the second electrode pair, only particle C was not deflected and traveled toward the bottom channel. Particles A and B were both deflected to the third electrode, where B was deflected again toward the center channel and A passed through into the top most channel.

The fourth and final stage of the integrated chip was used to trap and concentrate the particles as they were being sorted. Unlike an electrode straight across the channel,[20] we designed an electrode to optimally counter Stokes drag, and trap and concentrate the particles. As shown in the chip image in Fig. 1(c), the final electrodes in each channel have different shapes; an arrowhead, a crescent, and a flower. All trapping electrodes are tuned to the frequency that all the bacteria would exhibit nDEP to act as a gate and prevent the bacteria from passing through the electrode pair. However, due to the high flow rate, and the strength of the DEP force some bacteria would pass through the electrode. Therefore, the different electrode designs were used to test their

trapping efficiency. The crescent electrodes should slowly focus the particles toward the center, leaving large regions at the tip of the electrode for the particles to concentrate. The flower electrode, due to the multiple curves, should allow the particles to first trap in one curve, and as they slow down due to the nDEP force, the particles would concentrate in the final curve at the tip of the electrode. The arrowhead electrode was designed to focus the bacteria to the tip of the electrode and to trap at the sharp tip.

III. MATERIALS AND METHODS

A. Micro-electrode fabrication

Au/Cr electrodes (200 nm/50 nm thick) were deposited on a glass slide (Kimble, $76 \times 26 \times 1$ mm) by an electrobeam evaporator (E-beam VT1-10CE, ULVAC). Negative photoresist (AZ 5214) was spin-coated on the deposited metal layer and patterned by standard photolithography techniques with the electrode geometry. The metal layer was then etched and the remaining photoresist removed.

B. Micro-channel fabrication

After electrode patterning, each slide was cleaned by acetone and isopropanol. A photosensitive epoxy-based photoresist, SU 8-25 was spin-coated on one slide. Following standard lithography techniques of exposure and developing, a channel was patterned into the SU-8 with a height of 25 μm, a width of 1 mm, and a length of 14.5 mm. The three branch channels are 350 μm in width and 5.5 mm in length. The inlet and outlet holes were drilled by a diamond drill into a second electrode patterned slide.

A UV curable adhesive glue (LOCTITE 3491) with a viscosity of 900 Cp was spin-coated onto the slide with the SU 8 layer leaving a 3–5 μm thick coating of glue. When the glue was spin-coated on the chip, it did not enter the channel because of the surface tension of the glue. The two electrode slides were aligned by a microscope pressed together and exposed to UV to cure the bonding of the two slides together. After applying pressure, the adhesive layer was found to be less than 1 μm thick. To prevent the glue from entering the channel when pressure was applied to the two slides, a small groove was patterned on the outer edges of the desired channel to ensure none of the glue entered the channel. The common method used to bond slides with UV glue is to inject the glue into the chip edge and rely on capillary action to spread the glue. However, the channel is often contaminated by this method. By spinning the glue on the chip and fabricating a groove, contamination of the channel is prevented, allowing for a fast and clean bonding method. The fabrication process is illustrated in the schematic in Fig. 4.

IV. EXPERIMENTAL SETUP

An applied function generator (WAVETEK 195) was used to reach an output voltage range of 5 $mV_{p\text{-}p}$ to 20 $V_{p\text{-}p}$ with a frequency range of 0 to 16 MHz and can output four different signals simultaneously. The sample was injected continuously into the microchannel by a microsyringe pump through a Teflon tube. The experiment was observed through an inverted microscope (Olympus CH 40) and recorded by a CCD camera. A depiction of the experimental setup is shown in Fig. 5.

An additional microscope and imaging system was used, an Olympus 1X71 inverted microscope and an I-Speed CDU camera system (Olympus, USA). An applied function generator (Tektronix CFG 253) was used to reach voltages up to 20 $V_{p\text{-}p}$ and frequencies up to 3 MHz along with a second function generator (Agilent 33220A) that can to reach voltages up to 10 $V_{p\text{-}p}$ and frequencies up to 20 MHz. A Renishaw 2000 Raman microscope with a 514.5 nm laser and silver nanoparticles ($\sim$80 nm) made as described in the procedure by Lee and Meisel[49] were used for SERS detection.

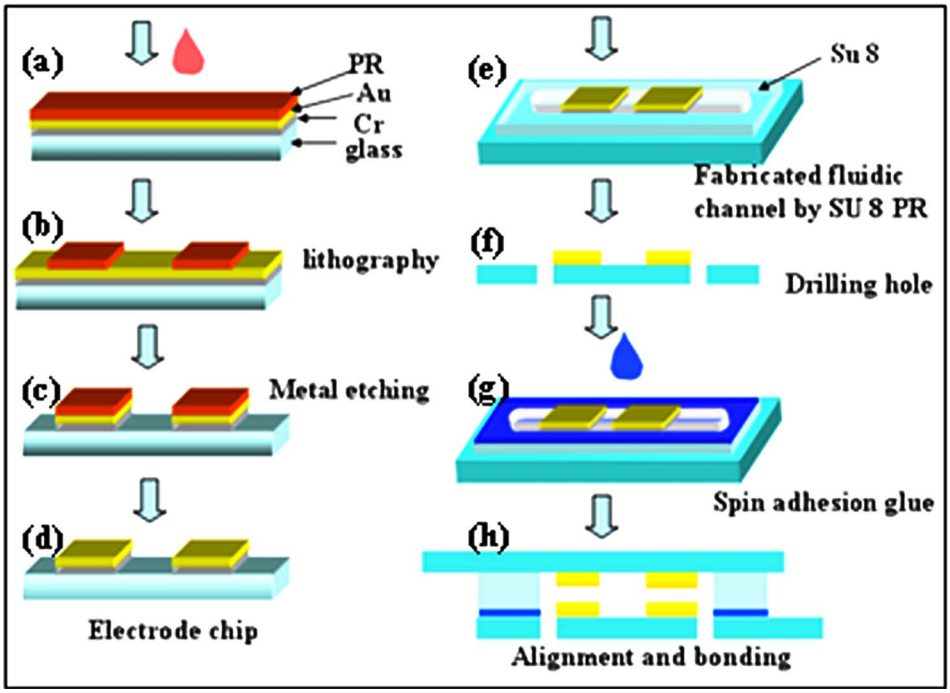

FIG. 4. Schematic of the chip process using standard lithography techniques.

A. Sample preparation

Fluorescent latex particles (Sigma-Aldrich, USA) ranging from 1 to 10 μm suspended in DI water at concentrations of 10^8 particles/ml were used for imaging each process of the integrated chip. *C. albicans* was obtained from the Department of Medical Laboratory Sciences and Biotech-

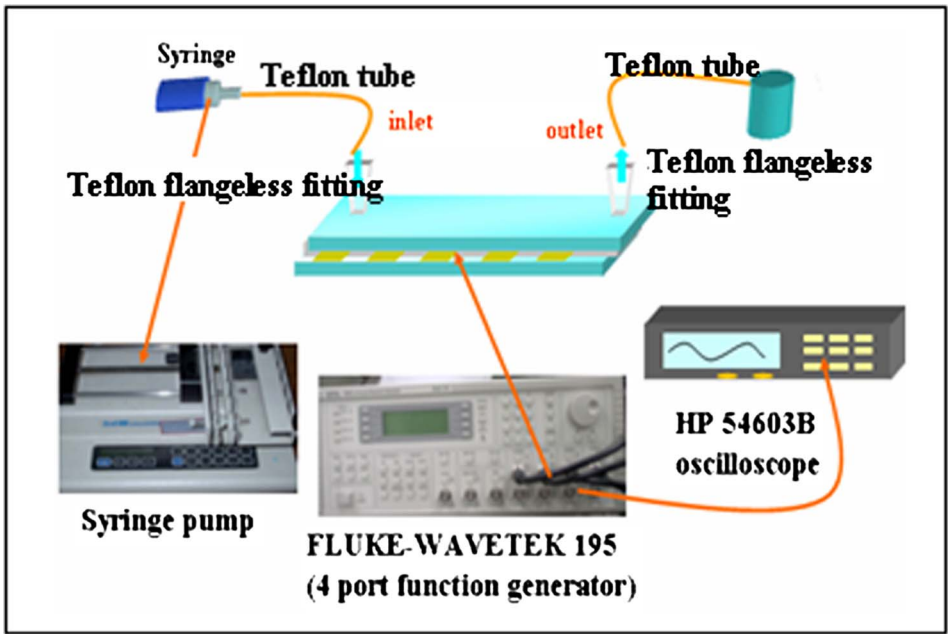

FIG. 5. Diagram of experimental set-up.

nology at the National Cheung Kung University in Tainan, Taiwan. The yeast sample was grown in SDA (Synthetic Defined Agar) for 48 h at 28 °C. The *C. albicans* was then suspended in a 10 mM KCl solution to reach a concentration of 10^8 colony forming units(CFU)/ml with a conductivity of 1405 μS/m. Heat killed *C. albicans* (100 °C, 20 min) were dyed with Trypan Blue and suspended in a 10 mM KCl solution. *E. coli Nissle* and the *Lactobacillus* were obtained from the University of Chicago Pritzker School of Medicine. The *E. coli* was grown in tryptic soy broth and *Lactobacillus* was grown in MRS (deMan Rogosa Sharpe) medium. Both bacteria were grown for 14 h at a temperature of 35 °C. Samples of 10^7 CFU/ml of each bacterium were suspended in a mixture of saline and D-mannitol (Sigma-Aldrich, USA) solution to reach conductivities ranging from 1200 μS/m to 1500 μS/m, as compared to the typical conductivity of 14 mS/m for saline solutions.

B. Methods

The DEP behaviors were first characterized by varying the frequencies from 500 kHz to 15 MHz at a fixed voltage to map the DEP properties. A highly concentrated solution of a single bacterium ($\sim 10^7$ CFU/ml) was placed on top of a planar electrode array as a drop and the motion of the bacteria was observed under an AC field. The trapping location of bacteria on the electrode edge or between the electrodes indicated whether the bacteria exhibited positive or negative DEP at that applied frequency. At low frequencies (<1 MHz) all the bacteria and the yeast exhibited nDEP in the conductive medium with conductivity beyond 1200 μS/m and were trapped in the electrode gaps. As the frequencies were increased, the bacteria reached their cross-over and were attracted to the electrode edges by pDEP. However, these preliminary cross-over frequency estimates were repeated within the chip under flow conditions, as detailed in the following section.

V. RESULTS AND DISCUSSION

A. DEP properties/filtering

The frequency ranges of nDEP and pDEP were experimentally determined for the *C. albicans*, *Lactobacillus*, and *E. coli Nissle*. A slow flow rate of 0.4 μL/min (linear velocity 0.1 mm/s) was used so that the bacteria would not pass through the filtering stage too fast for the DEP properties to be tested. At a voltage of 10 $V_{p\text{-}p}$, the frequency across the parallel electrodes was slowly increased until the DEP directions of the particles changed. The 1 μm latex particle exhibited pDEP at frequencies below 400 kHz and nDEP above this frequency. The 5 μm latex particles exhibited nDEP at all frequencies above 100 kHz for a suspension conductivity of 50 μS/m. The *E. coli* was found to exhibit strong nDEP at frequencies below 1 MHz and strong pDEP above 5 MHz, while *Lactobacillus* exhibited strong nDEP at frequencies below 1 MHz and strong pDEP properties above 10 MHz. The *C. albicans* was found to exhibit pDEP above 5 MHz at 18 $V_{p\text{-}p}$, while heat killed *C. albicans* stayed at nDEP through the entire frequency range. A mixture of live and dead *C. albicans* was passed through the filter under an applied field of 14 $V_{p\text{-}p}$ and a frequency of 10 MHz. The live cells were trapped at the filter electrodes, while the dead cells passed through the electrode array unaffected. The live *C. albicans* trapped on the parallel electrode are shown in Fig. 6(a).

B. Focusing

In the next stage of the chip, 2 μm fluorescent latex particles were seen being deflected toward the center of the channel, indicated by the light streak between the electrodes in both images of Figs. 6(b) and 6(c). These images are enhanced in the supplemental material. The particle velocity was roughly 1 mm/s through the channel under an applied voltage of 12 $V_{p\text{-}p}$ and a frequency of 10 MHz. The first set of focusing electrodes is shown in Fig. 6(b), where the particles are confined to a region of approximately 50 μm. However, there are multiple streaks, indicating that there were many particles passing through the gap between the focusing electrodes. In Fig. 6(c), the secondary focusing array of interdigitated electrodes are shown, where the par-

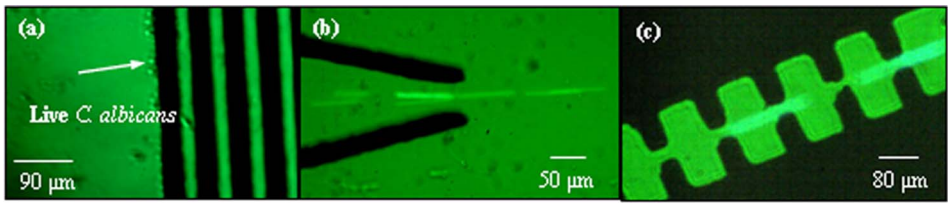

FIG. 6. Filtering and focusing stages of the chip with *C. albicans* and latex particles. (a) Filtering live/dead *C. albicans*, where live *C. albicans* exhibits pDEP at 10 MHz, 14 V_{p-p}, while dead *C. albicans* exhibits negative DEP and passes through the filtering array. (b) Focusing fluorescent 2 μm latex particles through the first focusing unit to a region of 50 μm. This image is enhanced in the supplemental material. (c) Finer focusing of the latex particles to a region of 20 μm (enhanced online).

ticles are confined to a much smaller area, and individual particles are seen passing through the electrode gap in a single line. This single-file queue for the particles is sustained in the remainder of the chip until the trapping stage. If debris filtering is unnecessary, the downstream focusing, sorting, and trapping can be done at a flow rate of 3 μL/min (linear velocity 1.5 mm/s). For a typical 100 μL sample, this corresponds to a processing time of 30 min.

C. Particle sorting

Recall that the DEP force scales as r^3, thus, larger particles will experience a stronger nDEP force than smaller particles and should therefore be deflected more readily. A mixture of 1 μm and 5 μm latex particles in an applied field of 8 V_{p-p} and 5 MHz was pumped through the chip. The 5 μm particles were indeed deflected by the sorting electrodes, while the 1 μm particles passed through the electrodes with only minor deflections. In Fig. 7(a), after the mixture of particles are focused to a single line, the 5 μm latex particles are seen to the left of the electrode pair, traveling along the length of the electrodes as they are deflected, while the 1 μm particles pass through the electrodes into a channel. This image is enhanced as a video in the supplemental material.

Along with sorting by size, different bacteria exhibit different DEP properties. In a 1500 μS/m solution at 15 V_{p-p} and 3.3 MHz, *Lactobacillus* has a strong nDEP force, while at the same frequency *E. coli* is near its cross-over frequency. The deflection due to the electrodes was minimal for the *E. coli* and was seen passing through the electrodes. *Lactobacillus* was deflected along the electrode like the 5 μm latex particles and continued through the channel after traveling the length of the electrodes, as seen in Fig. 7(b). Thus, the electrodes can be used to sort mixtures of bacteria into various channels and can be further scaled to accommodate a larger number of bacteria mixtures. With a linear particle velocity of 500 μm/s, this translates into about 500 particles being processed per second. This number is consistent with the product of the typical

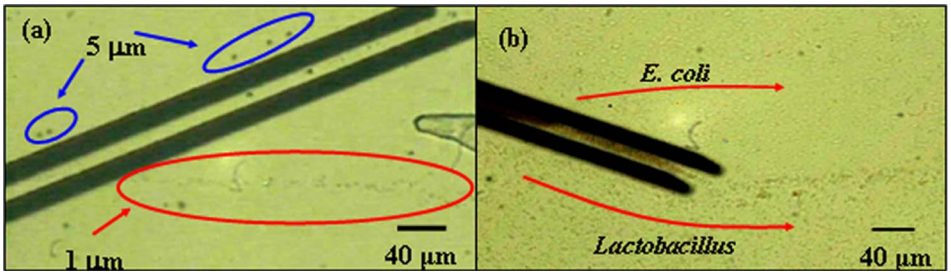

FIG. 7. Sorting latex particles and *Lactobacillus* based on their negative DEP mobilities. (a) A mixture of 1 and 5 μm latex particles are separated because the 5 μm latex particles exhibit strong nDEP mobilities at 5 MHz, and 8 V_{p-p} and are being deflected along the length of the electrode. This image is enhanced in the supplemental material. (b) The mixture of *Lactobacillus* and *E. coli Nissle* at 15 V_{p-p} and 3.3 MHz being separated, where the *Lactobacillus* is being deflected along the electrode while the *E. coli* pass through the electrode gate (enhanced online).

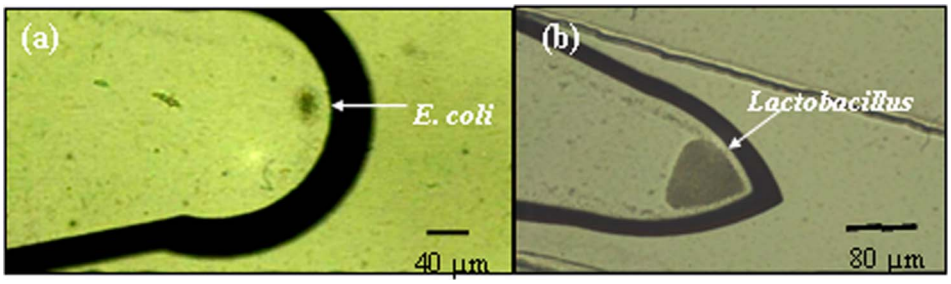

FIG. 8. Trapping of *E. coli* and *Lactobacillus* after they have been sorted into their individual channels. Under a field of 18 V_{p-p} and 500 kHz, both bacteria exhibit nDEP properties and are trapped and concentrated. (a) *E. coli* is trapped in the crescent electrode and (b) *Lactobacillus* is trapped in the arrowhead electrode. This image is enhanced in the supplemental material.

sample volume (100 μl) and bacteria concentration (10^7 CFU/ml) divided by the typical processing time (30 min).

D. Particle trapping

The final electrodes on the integrated chip were used to trap and concentrate the bacteria once they were separated into their individual channels. As the *E. coli* and *Lactobacillus* were being sorted, they were trapped in the arrowhead and the crescent electrode, respectively, as seen in Figs. 8(a) and 8(b). In both electrode designs a large fraction of the bacteria was trapped. However, the amount of *E. coli* trapped in the crescent electrode was considerably less than the *Lactobacillus*. The two different electrodes configurations were trapping at different rates as expected from the analysis of Fig. 2.

From the image of the chip in Fig. 1, three trapping electrode designs were used. However, only two designs were found to be effective in trapping and concentrating, the arrowhead and the crescent shaped electrode. The trapping rate for both of these configurations was rapid, as seen in the sequence of images of the crescent electrodes in Fig. 9, taken at 20 s intervals. This image is enhanced in the supplemental material to show the trapping rate of the arrowhead electrode. A sample of 10 μm latex particles was trapped with an applied field of 14 V_{p-p} at a frequency of 10 MHz. The particles can be seen being deflected by the electrode and directed toward the concentrated particles by the streaks in the image. However, particles can be seen passing through the electrodes, suggesting that the trapping electrode cannot prevent all the particles from passing

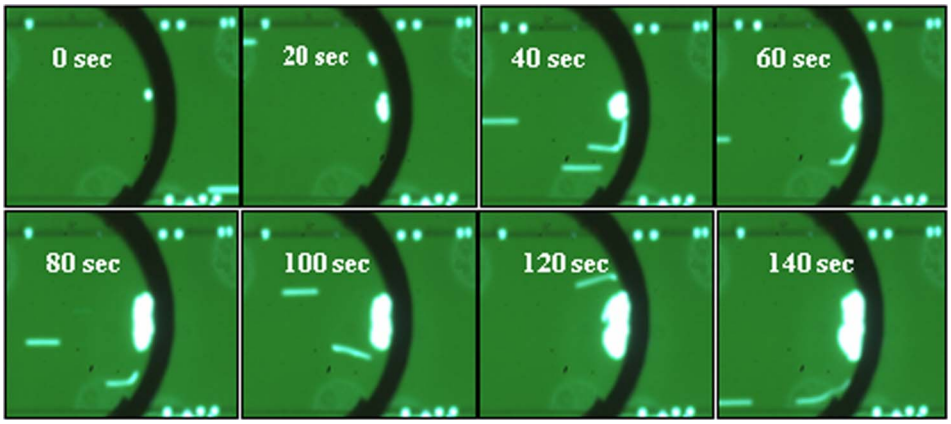

FIG. 9. Trapping rate of fluorescent 5 μm latex particles in the crescent electrode under an applied field of 14 V_{p-p} and 10 MHz over 2 min. Images were taken at 20 s intervals. This image is enhanced in the supplemental material to show the trapping rate of the arrowhead electrode (enhanced online).

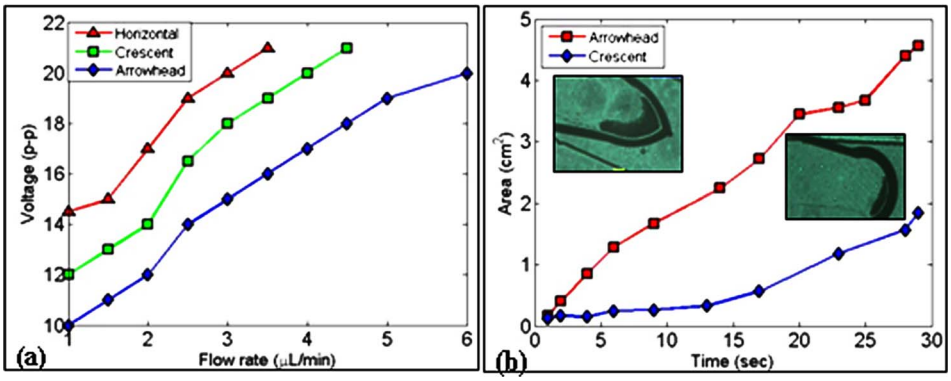

FIG. 10. Trapping efficiency comparing a horizontal electrode with the crescent and the arrowhead electrode at 19 V_{p-p} and 3 MHz. (a) The voltage at which each electrode can trap particles at varying flow rates is plotted. The arrowhead electrode can trap at lower voltages and higher flow rates due to the sharp tip of the electric field. The horizontal electrode can trap the least, requiring the highest voltage at low flow rates. (b) Comparing area of the concentrated particles once they are trapped by the crescent and the arrowhead electrode at a volume flow rate of 3 μL/min and a particle velocity of 2 mm/s. The arrowhead electrode has a larger area of trapped particles, letting the least amount of particle pass through the trapping electrode.

through the channel. This may be due to the particle-particle interaction and the varying vertical position of the particles. The trapping electrode regime can also become saturated with particles at high concentrations and prevent particles from trapping at the electrode. Once the particles have packed together at the trapping electrode and settled to the bottom, they will affect the flow above them and force the particles to flow higher in the channel and not through the optimal region of nDEP in the electrode gate.

The trapping efficiency of the two electrode designs was compared to a horizontal electrode gate. The flow rate and the voltage required to successfully trap particles using the crescent, arrowhead, and horizontal electrodes were measured and plotted in Fig. 10(a). As expected, the arrowhead electrode can trap at higher flow rates and at lower voltages. This is most likely due to the tip of the arrowhead because the sharp angle of the arrowhead electrode increases the electric field, as seen from the simulation in Fig. 2(b), allowing for a stronger nDEP effect on the particles. While the crescent electrode slowly curves the particles toward the center of the channel and the particles are seen to migrate toward the concentrated slug, the field at this tip is not as strong as the field due to a sharp angle.

Another criterion that is considered in the trapping efficiency of the electrodes, is the amount of particles that leak through the electrodes. 5 μm latex particles at a flow rate of 3.5 μL/min ($v=2$ mm/s) and 19 V_{p-p} were trapped in both the arrowhead and the crescent electrodes and the area of the particles trapped was measured over a time of 30 s. The resulting area versus time was plotted in Fig. 10(b). The horizontal electrode was not considered because it cannot trap at high flow rates. As can be seen in the images, the trapping area of the arrowhead electrode is much greater than that of the crescent, indicating that fewer particles were leaking through the arrowhead electrode. With the small channel height of 25 μm and a suspension consisting of 5 μm particles, the piling effect of the particles once they were stopped was relatively low and it occurred for both electrode systems. Thus, we can see that the arrowhead electrode is a better trapping electrode not only because it increases the field effect on the particles by the sharp electrode tip, but also utilizes the profile of the flow field to maximize the nDEP effect on the particles as it enters into the channel.

E. Detection

As the bioparticles were trapped at the crescent and arrowhead electrodes, a concentrated slug was found on the glass slide, as seen in the previous images. Within this slug, the concentration is extremely high and can be used for Raman detection. A mixture comprised of 300 μL of 80 nm

(a)

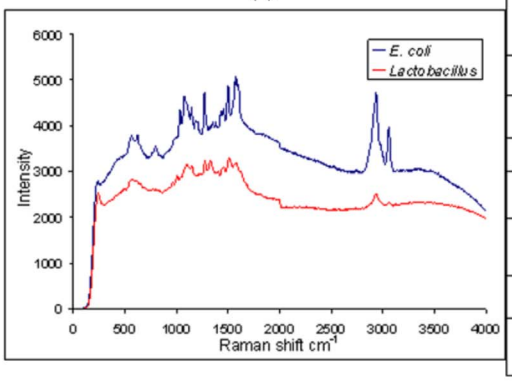

(b)

E. Coli Peaks (cm^{-1})	*Lactobacillus* Peaks (cm^{-1})	Corresponding Bonds
557	546	C-Br, C-I, C-Cl
1072	1082	Aromatic C=S
1140	1137	C=S
1449	1499	Aromatic Ring
1565	1560	Aromatic/hetero ring
2924	2923	C-CH_3
3050	3042	CH=CH, Aromatic C-H

FIG. 11. Raman spectra of *E. coli* and *Lactobacillus* using SERS. (a) The red line indicates the *Lactobacillus* "fingerprint" and the blue line is the *E. coli*. (b) A sample of their peaks and corresponding bonds.

silver nanoparticles and 1 mL of 10^7 CFU/ml of *E. coli* is trapped at the electrodes in an applied field of 14 $V_{p\text{-}p}$ at a frequency of 500 kHz. Focusing the laser onto the concentrated slugs through one of the glass slides of the enclosed chip, a Raman spectrum was taken of the concentrated slugs ~3 min after sorting commenced. The resulting spectrum of *E. coli* is shown in blue in Fig. 11(a) using an integration time of 100 s with one accumulation step. A similar experiment with the same conditions was used for obtaining the red spectrum of the *Lactobacillus* in Fig. 10. The two bacteria spectra have very distinct peaks and distinct spectra. A list of some of their similar peaks and possible corresponding bonds is shown in Fig. 11(b).[34] Current databases are still compiling Raman spectrum and characterization information on bacteria and other micro-organisms. Due to their complex exterior, there are many proteins and amino acids that are common in more cell walls and cell membranes. However, their interactions with other molecules, orientations, and quantities still differ in producing a very distinct and different Raman spectra. Thus, the integrated chip is equipped to accommodate Raman detection of the bacteria and can be used as a quantification and identification method with the concentrated slug at the traps.

VI. CONCLUSIONS

We have fabricated a continuous integrated chip that can filter, focus, sort, and trap heterogeneous bioparticle and colloid populations on a single chip at a rate of 500 particles/s. These processes were achieved with 3D electrode gates that utilize different nDEP mobilities of the bacteria and other particles in a high-conductivity buffer to manipulate them within the channel. The trapping electrode utilized a special design that exploits the strength of the electric field at sharp electrode corners and the low flow rate at the side of the channels. The arrowhead electrode design was found to be the most effective in trapping and concentrating particles at a high velocity of 1.5 mm/s. We have successfully sorted and concentrated a sepsis-causing yeast, *C. albicans*, and two gastrointestinal bacteria, *E. coli Nissle* and *Lactobacillus*, and have identified the latter two by Raman spectroscopy. Sorting and identification can be done in less than 50 min for a 100 μl sample. This rapid sorting of a large volume of sample suggests that the chip can be scaled up to accommodate finer sorting into more bins than three and that a much more complex matrix can be processed at higher efficiencies with recycling or higher number of sorting and filtering stages. Trapped particles can also be released in stages to examine different particles with cross-over frequencies over a wide range. These massively parallel chips are currently being pursued in our laboratories.

ACKNOWLEDGMENTS

The authors would like thank Dr. Eugene Chang at the University of Chicago Medical School for supplying the gastrointestinal bacteria cultures and Professor Tsung-Chain Chang in the Department of Medical Laboratory Sciences and Biotechnology at the National Cheung Kung University, Tainan, Taiwan for supplying the sepsis yeast cultures. Additionally, the authors thank Dr. G. N. R. Tripathi and Vadim Kagan of the Notre Dame Radiation Laboratory for their support with the Renishaw Raman microscope and for providing the suspensions of silver nanoparticles. The authors also acknowledge Dr. Shramik Sengupta for culturing the *E. coli* and *Lactobacillus* used in these experiments. Diana Hou and Hsueh-Chia Chang are supported by NSF Grant No. CT504-54956 and NASA Grant No. NAG5-10503, along with a Bayer Fellowship. I-Fang Cheng and Hsien-Chang Chang are supported by the NSC Grant No. 94-2320-B-006-031.

[1] G.-B. Lee, B.-H. Hwei, and G.-R. Huang, J. Micromech. Microeng. **11**, 654 (2001).
[2] A. Minerick, P. Takhistov, R. Zhou, and H.-C. Chang, Electrophoresis **24**, 3703 (2003).
[3] M. P. Hughes, Electrophoresis **23**, 2569 (2002).
[4] M. P. Hughes, H. Morgan, F. J. Rixon, J. Burt, and R. Pethig, Biochim. Biophys. Acta **1425**, 119 (1998).
[5] H. A. Pohl, *Dielectrophoresis* (Cambridge University Press, London, 1978).
[6] W. M. Arnold, IEEE Trans. Ind. Appl. **37**, 1468 (2001).
[7] Z. Gagnon and H.-C. Chang, Electrophoresis **26**, 3725 (2005).
[8] X.-F. Zhou, G. H. Markx, R. Pethig, and I. M. Eastwood, Biochim. Biophys. Acta **1245**, 85 (1995).
[9] K. L. Chan, H. Morgan, E. Morgan, I. T. Cameron, and M. R. Thomas, Biochim. Biophys. Acta **1500**, 313 (2000).
[10] G. H. Markx, P. A. Dyda, and R. Pethig, J. Biotechnol. **51**, 175 (1996).
[11] H. Li and R. Bashir, Sens. Actuators B **86**, 215 (2002).
[12] X. B. Wang, J. Yang, Y. Huang, J. Vykoukal, F. F. Becker, and P. R. Gascoyne, Anal. Chem. **72**, 832 (2000).
[13] S. Choi and J.-K. Park, Lab Chip **5**, 1161 (2005).
[14] I. Doh and Y.-H. Cho, Sens. Actuators, A **121**, 59 (2005).
[15] M. Yamada, M. Nakashima, and M. Seki, Anal. Chem. **76**, 5465 (2004).
[16] G. H. Markx and R. Pethig, Biotechnol. Bioeng. **45**, 337 (1995).
[17] J. Wu, Y. Ben, D. Battigelli, and H.-C. Chang, Ind. Eng. Chem. Res. **44**, 2815 (2005).
[18] N. G. Green, H. Morgan, and J. J. Milner, J. Biochem. Biophys. Methods **35**, 89 (1997).
[19] T. Muller, G. Gradl, S. Howitz, S. Shirley, Th. Schnelle, and G. Fuhr, Biosens. Bioelectron. **14**, 247 (1999).
[20] C. D. James, M. Okandan, P. Galambos, S. S. Mani, D. Bennett, B. Khusid, and A. Acrivos, J. Fluids Eng. **128**, 14 (2006).
[21] S. Fielder, S. G. Shirley, T. Schnelle, and G. Fuhr, Anal. Chem. **70**, 1909 (1998).
[22] D. J. Bennett, B. Khusid, C. D. James, P. C. Balambos, M. Okandan, D. Jacqmin, and A. Acrivos, Appl. Phys. Lett. **83**, 4866 (2003).
[23] T. Schnelle, T. Muller, S. Fielder, and G. Fuhr, J. Electrost. **46**, 13 (1999).
[24] Y. Li, C. Dalton, H. J. Crabtree, G. Nilsson, and K. V. I. S. Kaler, Lab Chip **7**, 239 (2006).
[25] H. Morgan, D. Holmes, and N. G. Green, IEE Proc.: Nanobiotechnol. **150**, 76 (2003).
[26] D. Holmes, H. Morgan, and N. G. Green, Biosens. Bioelectron. **21**, 1621 (2006).
[27] J. Suehiro, A. Ohtsubo, T. Hatano, and M. Hara, Sens. Actuators B **119**, 319 (2006).
[28] R. Zhou, P. Wang, and H.-C. Chang, Electrophoresis **27**, 1376 (2006).
[29] J. C. Liao, M. Mastali, V. Gau, M. A. Suchard, A. K. Moller, D. A. Bruckner, J. T. Babbitt, Y. Li, J. Gornbein, E. M. Landaw, E. R. B. McCabe, B. M. Churchill, and D. A. Haake, J. Clin. Microbiol. **44**, 561 (2006).
[30] E. T. Lagally, S.-H. Lee, and H. T. Soh, Lab Chip **5**, 1053 (2005).
[31] T. Vo-Dinh, F. Yan, and M. B. Wabuyele, J. Raman Spectrosc. **36**, 640 (2005).
[32] Q. Wu, T. Hamilton, W. H. Nelson, S. Elliott, J. F. Sperry, and M. Wu, Anal. Chem. **73**, 3432 (2001).
[33] M. Kummerle, S. Scherer, and H. Seiler, Appl. Environ. Microbiol. **64**, 2207 (1998).
[34] E. Smith and G. Dent, *Modern Raman Spectroscopy: A Practical Approach* (John Wiley & Sons, West Sussex, England 2005).
[35] R. M. Jarvis and R. Goodacre, Anal. Chem. **76**, 40 (2004).
[36] G. J. Thomas, Jr., Annu. Rev. Biophys. Biomol. Struct. **28**, 1 (1999).
[37] B. W. D. de Jong, T. C. Bakker Schut, K. Maquelin, T. vander Kwast, C. H. Bangma, D.-J. Kok, and G. J. Puppels, Anal. Chem. **78**, 7761 (2006).
[38] Y. C. Cao, R. Jin, and C. A. Mirkin, Science **297**, 1536 (2002).
[39] K. Kneipp, H. Kneipp, I. Itzkan, R. R. Dasari, and M. S. Feld, J. Phys.: Condens. Matter **14**, R597 (2002).
[40] R. Petry, M. Schmitt, and J. Popp, ChemPhysChem **4**, 15 (2003).
[41] R. M. Jarvis, A. Brooker, and R. Goodacre, Faraday Discuss. **132**, 281 (2006).
[42] F. Yan, M. B. Wabuyele, G. D. Griffin, A. A. Vass, and T. Vo-Dinh, IEEE Sens. J. **5**, 665 (2005).
[43] C. J. Orendorff, A. Gole, T. K. Sau, and C. J. Murphy, Anal. Chem. **77**, 3261 (2005).
[44] T. Vo-Dinh, D. L. Stokes, G. D. Griffin, M. Volkan, U. J. Kim, and M. I. Simon, J. Raman Spectrosc. **30**, 785 (1999).
[45] W. R. Premasiri, D. T. Moir, M. S. Klempner, N. Krieger, G. Jones II, and L. D. Ziegler, J. Phys. Chem. B **109**, 312 (2005).

[46] S. K. Thamida and H.-C. Chang, Phys. Fluids **14**, 4315 (2002).
[47] N. Flores-Rodriguez and G. H. Markx, J. Micromech. Microeng. **16**, 349 (2006).
[48] M. Durr, J. Kentsch, T. Muller, T. Schnelle, and M. Stelzle, Electrophoresis **24**, 722 (2003).
[49] P. C. Lee and D. Meisel, J. Phys. Chem. **86**, 3391 (1982).